Available online at www.sciencedirect.com
SCIENCE DIRECT
International Journal of Heat and Mass Transfer 49 (2006) 3785–3799
International Journal of HEAT and MASS TRANSFER
www.elsevier.com/locate/ijhmt

Heat transfer behavior in the impingement zone under circular water jet

Fuchang Xu, Mohamed S. Gadala *

Department of Mechanical Engineering, The University of British Columbia, 2324 Main Mall, Vancouver, BC, Canada V6T-1Z4

Received 26 October 2005; received in revised form 30 March 2006
Available online 14 June 2006

Abstract

In this study an iterative and sequential inverse heat transfer analysis procedure is developed and implemented into a two-dimensional finite element program. The developed program is used to determine the heat fluxes at the stagnation points of stationary hot plates cooled by impingement water jets in an industry scale test facility. Analysis of data shows that the heat transfer behavior at the stagnation is mainly affected by water temperature and hardly affected by water flow rate with mild effect from steel grade. The features of boiling curves and the typical values obtained are in good agreement with data in the literature.

Keywords: Inverse heat conduction; Water jet cooling; Finite element method

1. Introduction

Steel strip is one of the most versatile hot rolled products with a wide variety of applications ranging from automobile bodies to drink can [1]. While the geometry and surface quality of steel strips are mainly influenced by the rolling deformation procedures, microstructure and mechanical properties highly depend on the controlled cooling procedure on the runout table (ROT). During the specially designed controlled cooling, the cooling start and finish temperatures and the cooling rate are exercised accurately according to the expected property in terms of phase composition, size and distribution.

In order to successfully realize the controlled cooling process on ROT, it is crucial to get the accurate heat transfer coefficient or heat flux value and its distribution along the length and the width of the plate. The first step hereby is to investigate the heat transfer phenomena of stationary hot plate under a single circular jet which is an essential component of the cooling system used in ROT.

Numerous researches, both experimental and/or numerical, have been performed on the subject of water jet cooling [2–16]. This prior research work has constituted insight into the water jet cooling on ROT but there are still to some extent many important points to be examined. Many research results in the literature address the jet impingement problem under the steady state conditions, i.e., the test specimens were constantly heated while being cooled by water impinging jet. As for the tests using transient conditions, the dimensions of nozzles, the distance of nozzle to plate are quite small and/or the plate temperatures are low and may not reflect those used in the industrial practice on ROT. The results of such research effort have been important in providing insight into the problem but, generally, were difficult to apply to practical situations on ROT.

In the analysis and simulation side, various inverse heat conduction methods have been developed to evaluate heat flux or heat transfer coefficient on a heated or cooled surface [17–21]. The advantage of using inverse method is that only the temperatures measured at some proper internal locations of the test plate are required. Research work also showed that the uniqueness and stability of an inverse heat conduction problem (IHCP) solution could be assured if

* Corresponding author. Tel.: +1 604 822 2777; fax: +1 604 822 2403.
E-mail address: gadala@mech.ubc.ca (M.S. Gadala).

0017-9310/$ - see front matter © 2006 Published by Elsevier Ltd.
doi:10.1016/j.ijheatmasstransfer.2006.03.034

some techniques are adopted even though the IHCP would be typically ill-posed and would normally be sensitive to the measurement errors.

This paper presents the following work:

(1) A FEM-based iterative and sequential algorithm and program for IHCP.
(2) The experimental setup, a ROT test facility of industrial scale constructed at the University of British Colombia (UBC), and the impingement cooling tests using one circular water jet [21–24].
(3) The heat fluxes in impingement zone, and the effects of processing parameters such as water temperature, water flow rate on the predicted fluxes.

2. Numerical modeling

The modeling and experimental procedures are based on 2D planar and axisymmetric assumption. For completeness of the treatment, a brief outline of the equations for direct FE formulation of transient conduction heat transfer problem is given in the following section. Detailed account of such formulation may be found in Ref. [25].

2.1. Formulation for direct analysis

The general governing equation for 2D conduction heat transfer problems, shown in Fig. 1, is written in the form:

$$\frac{\partial}{\partial x}\left(k_x\frac{\partial T}{\partial x}\right)+\frac{\partial}{\partial y}\left(k_y\frac{\partial T}{\partial y}\right)+\mathbf{q}^{\mathrm{b}}=c_p\rho\frac{\partial T}{\partial t} \tag{1}$$

where T is the temperature, °C; $\mathbf{q}^{\mathrm{b}}$ is the heat generation per unit volume, W/m^3; k_x and k_y are the conductivities in the x- and y-directions, respectively, W/m °C; ρ is the density, kg/m^3; c_p is the specific heat, J/kg °C; t is the time, s; and x, y are the Lagrangian coordinates of point.

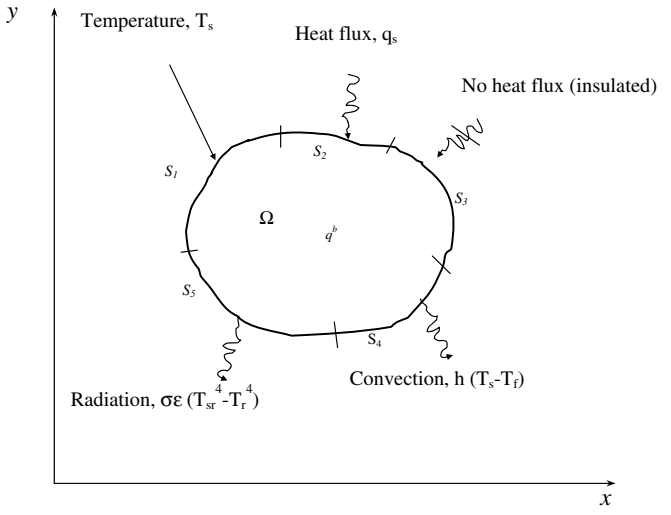

Fig. 1. General conduction heat transfer.

The boundary conditions may be one or a combination of the followings cases:

Prescribed temperature. This is an example of *Dirichlet* boundary condition (BC). The prescribed temperature T_{s} (°C) may be function of time and boundary coordinate (spatial function):

$$T=T_{\mathrm{s}}(x,y,t)\quad\text{on } S_1 \tag{1.a}$$

Prescribed heat flux. Specified heat flux (q_{s}) may be spatial function or function of time:

$$-\left(k_x\frac{\partial T}{\partial x}+k_y\frac{\partial T}{\partial y}\right)=q_s(x,y,t)\quad\text{on } S_2 \tag{1.b}$$

where q_{s} is the specified rate of heat flow per unit area (W/m^2). Prescribed heat flux is an example of Cauchy's or Neumann BC. If q_{s} is zero, it will represent a natural BC.

Convection heat exchange. When there is a convective heat transfer on part of the body surface, S_4, due to contact with a fluid medium, we have:

$$-\left(k_x\frac{\partial T}{\partial x}+k_y\frac{\partial T}{\partial y}\right)=h(T_{\mathrm{s}}-T_{\mathrm{f}})\quad\text{on } S_4 \tag{1.c}$$

where h is the convection heat transfer or film coefficient (W/m^2 °C), which may be temperature dependent (nonlinear), T_{s} is the surface temperature (°C) on S_4 and T_{f} is the fluid temperature (°C), which may be spatial or time function.

Radiation. Assuming grey body, the BC is given by:

$$-\left(k_x\frac{\partial T}{\partial x}+k_y\frac{\partial T}{\partial y}\right)=\varepsilon\sigma[T_{\mathrm{sr}}^4-T_{\mathrm{r}}^4]\quad\text{on } S_5 \tag{1.d}$$

where ε is the emissivity of the surface of the body, σ is the Stefan–Boltzmann constant (W/m^2 K^4), T_{sr} is the absolute temperature of surface S_5 (K) and T_{r} is the known absolute temperature of the external radiative source (K). The radiation boundary condition may be dealt with as a nonlinear convective boundary condition with an equivalent temperature dependent film coefficient, κ, where:

$$\kappa=\varepsilon\sigma(T_{\mathrm{sr}}^2+T_{\mathrm{r}}^2)(T_{\mathrm{sr}}+T_{\mathrm{r}}) \tag{1.e}$$

Using a weighted residual Galerkin procedure, the final finite element equations may be written as:

$$\mathbf{C}\dot{\mathbf{T}}+\mathbf{K}\mathbf{T}=\mathbf{Q} \tag{2}$$

where $\mathbf{C}$ is the equivalent heat capacity matrix, $\mathbf{K}$ is the equivalent heat conduction matrix, $\mathbf{T}$ and $\dot{\mathbf{T}}$ are vectors of the nodal temperature and its derivatives, respectively, and $\mathbf{Q}$ is the equivalent load vector.

A general family of solution algorithms for Eq. (2) may be obtained by introducing a parameter α where $0.0\leqslant\alpha\leqslant 1.0$ such that

$${}^{t+\alpha\Delta t}\dot{\mathbf{T}}=\frac{1}{\Delta t}({}^{t+\Delta t}\mathbf{T}-{}^{t}\mathbf{T})=\frac{1}{\alpha\Delta t}({}^{t+\alpha\Delta t}\mathbf{T}-{}^{t}\mathbf{T}) \tag{3}$$

$${}^{t+\alpha\Delta t}\mathbf{T}=\alpha{}^{t+\Delta t}\mathbf{T}+(1-\alpha){}^{t}\mathbf{T} \tag{4}$$

If $\alpha=0$ an explicit Euler forward method is obtained; if $\alpha=1/2$ an implicit trapezoidal rule is obtained; and if

$\alpha = 1$ an implicit Euler backward method is obtained. Substituting Eq. (3) into Eq. (2) and applying Newton–Raphson iterations yields:

$$^{t+\alpha\Delta t}\left[\mathbf{K}+\left(\frac{1}{\alpha\Delta t}\right)\cdot\mathbf{C}\right]^{(i-1)}\Delta\mathbf{T}^{(i)} = {}^{t+\alpha\Delta t}(\mathbf{Q}^b+\mathbf{Q}^s)+{}^{t+\alpha\Delta t}(\widehat{\mathbf{Q}}^h+\widehat{\mathbf{Q}}^r)^{(i-1)}-{}^{t+\alpha\Delta t}(\widehat{\mathbf{Q}}^c+\hat{\mathbf{q}}^c)^{(i-1)} \tag{5}$$

where $\alpha \neq 0$ and the definition of all terms is given in Appendix A. All quantities at time $(t+\alpha\Delta t)$ are calculated from a relation similar to Eq. (4).

Depending on the value of α, the procedure may be either conditionally stable ($\alpha < 0.5$) or unconditionally stable $\alpha \geqslant 0.5$.

Nonlinearities may arise from the dependence of thermo-physical properties on temperature as for the case of radiation boundary condition. In the developed program, nonlinearities are handled in step-wise staggered approach, i.e., the values of parameters at the current step are calculated out based on the temperature at the previous step and are assumed to be constant during the current step. The heat generation due to phase transformation may be treated in a similar manner.

2.2. Formulation for inverse analysis

2.2.1. Basic concepts

An IHCP may be generally converted to an optimization problem. The objective function of the optimization problem may be considered as the sum of the squares of the differences between calculated and measured temperatures. Due to the fact that inverse problems are generally ill posed, the solution to the IHCP may not be unique and would be normally sensitive to measurement errors. To reduce such sensitivity and improve the simulation, a number of future time steps (n_{FTS}) are employed in the analysis of the current step. This means that in addition to the measured temperature at the current time step $\mathbf{T}^i$, the measured temperatures at future time steps $\mathbf{T}^{i+1}$, $\mathbf{T}^{i+2},\ldots,\mathbf{T}^{i+n_{\mathrm{FTS}}}$ are also employed to estimate the heat flux $\mathbf{q}^i$.

In the above process, a temporary assumption would be normally considered for the values of $\mathbf{q}^{i+1},\mathbf{q}^{i+2},\ldots,\mathbf{q}^{i+n_{\mathrm{FTS}}}$ and is normally called function specification. The simplest and most widely used one is to use $\mathbf{q}^{i+k}=\mathbf{q}^i$, for $1 \leqslant k \leqslant n_{\mathrm{FTS}}$. The function specification technique works as a regularization procedure which stabilize the solution process.

To damp the fluctuation of solution due to measurement error, the objective function may be made more extensive by including more variables in the expression. A commonly used variable in this regard is some scalar quantity based on the heat flux vector $\mathbf{q}$, which may be employed with some kind of a weighting factor α that is normally called the regularization parameter. Higher order regularization parameters involving spatial derivatives of $\mathbf{q}$ are normally not adopted. This may be due to the fact that heat fluxes in water jet impingement cooling may dramatically change in space.

2.2.2. Calculation of heat flux

Based on the above discussion, an objective function in the least-squares method with sequential function specification and regularization may be expressed as follows:

$$F(\mathbf{q}) = \sum_{i=1}^{N}(\mathbf{T}_{\mathrm{m}}^i-\mathbf{T}_{\mathrm{c}}^i)^{\mathrm{T}}(\mathbf{T}_{\mathrm{m}}^i-\mathbf{T}_{\mathrm{c}}^i)+\alpha\sum_{i=1}^{N}\mathbf{q}^{iT}\mathbf{q}^i \tag{6}$$

where $\mathbf{T}_{\mathrm{m}}^i$, $\mathbf{T}_{\mathrm{c}}^i$ are the experimentally measured and the theoretically calculated temperature vectors at the ith time step, respectively, $\mathbf{q}^i$ is the heat flux vector at the ith time step, α is regularization factor and N is the number of total steps considered.

The heat flux and temperature vectors are

$$\mathbf{q} = [\,\mathbf{q}^1 \quad \mathbf{q}^2 \quad \ldots \quad \mathbf{q}^N\,]^{\mathrm{T}} \tag{7a}$$

$$\mathbf{q}^i = [\,q_1^i \quad q_2^i \quad \ldots \quad q_J^i\,]^{\mathrm{T}} \tag{7b}$$

$$\mathbf{T}_{\mathrm{m}}^i = [\,T_{1m}^i \quad T_{2\mathrm{m}}^i \quad \ldots \quad T_{L\mathrm{m}}^i\,]^{\mathrm{T}} \tag{8}$$

$$\mathbf{T}_{\mathrm{c}}^i = [\,T_{1\mathrm{c}}^i \quad T_{2\mathrm{c}}^i \quad \ldots \quad T_{L\mathrm{c}}^i\,]^{\mathrm{T}} \tag{9}$$

where L is the number of measurement points, J is the number of heat flux components that can be determined for flux space distribution on surface. It should be noted that J must be less than or equal to L, the number of measurement points. It should be noted that the dimensions of the heat flux vector $\mathbf{q}^i$ at each step is $1\times J$ while the total heat flux vector $\mathbf{q}$ is $J\times N$ as it includes the data in N steps, and the temperature vector $\mathbf{T}^i$ at each step is $1\times L$.

Eq. (6) may be written as

$$F(\mathbf{q}) = \sum_{i=1}^{N}(\mathbf{T}_{\mathrm{m}}^i-\mathbf{T}_{\mathrm{c}}^i)^{\mathrm{T}}(\mathbf{T}_{\mathrm{m}}^i-\mathbf{T}_{\mathrm{c}}^i)+\alpha\mathbf{q}^{\mathrm{T}}\mathbf{q} \tag{10}$$

It should be noted that the temperature $\mathbf{T}^k$ would be determined or affected only by the heat fluxes $\mathbf{q}^m$ where $m \leqslant k$. Mathematically we may express $\mathbf{T}^k$ as an implicit function of the heat flux:

$$\mathbf{T}_{\mathrm{c}}^k = f(\mathbf{q}^1,\mathbf{q}^2,\ldots,\mathbf{q}^k) \tag{11a}$$

or in a successive form as:

$$\begin{aligned}\mathbf{T}_{\mathrm{c}}^k &= f(\mathbf{T}_{\mathrm{c}}^{k-1},\mathbf{q}^k)\\ \mathbf{T}_{\mathrm{c}}^{k-1} &= f(\mathbf{T}_{\mathrm{c}}^{k-2},\mathbf{q}^{k-1})\\ &\vdots\\ \mathbf{T}_{\mathrm{c}}^{2} &= f(\mathbf{T}_{\mathrm{c}}^{1},\mathbf{q}^{2})\\ \mathbf{T}_{\mathrm{c}}^{1} &= f(\mathbf{T}_{\mathrm{c}}^{0},\mathbf{q}^{1})\end{aligned} \tag{11b}$$

and the following equation is valid:

$$\mathbf{T}_{\mathrm{c}}^k = \mathbf{T}_{\mathrm{c}}^{k^*}+\frac{\partial\mathbf{T}_{\mathrm{c}}^1}{\partial\mathbf{q}^1}(\mathbf{q}^1-\mathbf{q}^{1^*})+\frac{\partial\mathbf{T}_{\mathrm{c}}^2}{\partial\mathbf{q}^2}(\mathbf{q}^2-\mathbf{q}^{2^*})+\cdots + \frac{\partial\mathbf{T}_{\mathrm{c}}^k}{\partial\mathbf{q}^k}(\mathbf{q}^k-\mathbf{q}^{k^*}) \tag{12}$$

The values with a '*' superscript in Eq. (12) may be considered as initial guess values that would ultimately lead the temperature $\mathbf{T}_c^{k^*}$.

Now we define the first derivative of temperature $\mathbf{T}_c^i$ with respect to heat flux $\mathbf{q}^i$ as the sensitivity matrix:

$$\mathbf{X}^i = \frac{\partial \mathbf{T}_c^i}{\partial \mathbf{q}^i} = \begin{bmatrix} a_{11}(i) & a_{12}(i) & \dots & a_{1J}(i) \\ a_{21}(i) & a_{22}(i) & \dots & a_{2J}(i) \\ \vdots & \vdots & \ddots & \vdots \\ a_{L1}(i) & a_{L2}(i) & \dots & a_{LJ}(i) \end{bmatrix} \tag{13}$$

$$a_{rs}(i) = \frac{\partial T_{\mathrm{cr}}^i}{\partial \mathbf{q}_s^i}$$

where $i = 1, 2, \dots, N$, $r = 1, 2, \dots, L$ and $s = 1, 2, \dots, J$. The sensitivity matrix $\mathbf{X}^i$ is an $L \times J$ matrix.

The optimality of the objective function may be obtained by letting $\partial F/\partial \mathbf{q} = 0$ and we get the following set of equations (note that $\partial F/\partial \mathbf{q}$ should be done with respect to each component $\mathbf{q}^i$, with $i = 1, 2, \dots, N$):

$$\left\{ \sum_{i=1}^{N} \left(\frac{\partial \mathbf{T}_c^i}{\partial \mathbf{q}^j} \right)^T_{\mathbf{q}^j = \mathbf{q}^{j^*}} \left(\frac{\partial \mathbf{T}_c^i}{\partial \mathbf{q}^j} \right)_{\mathbf{q}^j = \mathbf{q}^{j^*}} + \alpha \mathbf{I} \right\} (\mathbf{q}^j - \mathbf{q}^{j^*}) = \sum_{i=1}^{N} \left(\frac{\partial \mathbf{T}_c^i}{\partial \mathbf{q}^j} \right)^T_{\mathbf{q}^j = \mathbf{q}^{j^*}} (\mathbf{T}_m^i - \mathbf{T}_c^{i^*}) - \alpha \mathbf{q}^{j^*} \quad j = 1, 2, \dots, N \tag{14}$$

where $\mathbf{q}^{j^*}$ is the initial guess of heat fluxes, $\mathbf{T}_c^{i^*}$ is the calculated temperature vector with the initial guess values.

Recalling Eqs. (12) and (13), Eq. (14) may be rearranged and written in the following form:

$$(\mathbf{X}^T_{\mathbf{q}=\mathbf{q}^*} \mathbf{X}_{\mathbf{q}=\mathbf{q}^*} + \alpha \mathbf{I})(\mathbf{q} - \mathbf{q}^*) = \mathbf{X}^{\mathrm{T}} \Delta \mathbf{T} - \alpha \mathbf{q}^* \tag{15}$$

where $\mathbf{X}$ is labelled as the total sensitivity matrix for multi-dimensional problem and has the following form:

$$\mathbf{X} = \begin{bmatrix} \mathbf{X}^1 & 0 & 0 & 0 \\ \mathbf{X}^2 & \mathbf{X}^1 & 0 & 0 \\ \vdots & \vdots & \ddots & 0 \\ \mathbf{X}^N & \dots & \mathbf{X}^2 & \mathbf{X}^1 \end{bmatrix} \tag{16}$$

and

$$\Delta \mathbf{T} = \begin{pmatrix} \mathbf{T}_m^1 - \mathbf{T}_c^{1^*} & \mathbf{T}_m^2 - \mathbf{T}_c^{2^*} & \dots & \mathbf{T}_m^N - \mathbf{T}_c^{N^*} \end{pmatrix}^{\mathrm{T}} \tag{17}$$

It should be noted that the dimension of matrix $\mathbf{X}$ is $(L \times N) \times (J \times N)$ and $\Delta \mathbf{T}$ has dimensions of $(L \times N)$. Also, it is worth noting that performing the calculation in Eq. (15) may be easily done in the time domain and no function specification for $\mathbf{q}^i$ is needed. If the total sensitivity is known, no iteration is required to get a final solution.

2.2.3. Iterative and sequential algorithms

2.2.3.1. Function specification and iteration technique. A perturbation algorithm [22] was used to obtain the sensitivity matrices $\mathbf{X}^1$ (only the information at current step was included in the work presented in [22]). First, a given value $\mathbf{q}^{1^*}$ is assumed for all components of the heat flux vector $\mathbf{q}^1$ as input in the direct heat transfer calculation to get the temperature distribution, say $\mathbf{T}_0^1$, for the given future steps at each thermocouple location. Then, one of the components, say J component, of heat flux $\mathbf{q}^1$ is increased a reasonable amount such as 10% to obtain new temperatures, $\mathbf{T}_J^1$. The ratios of temperature difference at each thermocouple location to the difference of heat flux component J are the sensitivity coefficients. Such perturbation is repeated for each component of the heat flux $\mathbf{q}^{1^*}$ until all sensitivity matrix components of $\mathbf{X}^1$ are obtained.

The above method would be adopted in this study. By applying this approach, several issues should be resolved. First, the heat fluxes $\mathbf{q}^{i^*}$ for $i = 2, \dots, N$ in the consecutive steps should be assigned. As mentioned in Section 2.2.1, function specification would stabilize the solution process. Moreover, it would simplify the calculation of the total sensitivity matrix $\mathbf{X}$. We hereby use a constant assumption, i.e. $\mathbf{q}^{1+k^*} = \mathbf{q}^{1^*} = \mathbf{q}^*$ for $1 \leqslant k \leqslant n_{\mathrm{FTS}}$. Therefore, all sensitivity matrices $\mathbf{X}^i$ for $i = 1, 2, \dots, N$ may be obtained from the above method by one assignment when the direct calculation is performed for N steps.

The second issue is the nonlinearity. The whole sensitivity matrix $\mathbf{X}$ is independent of the heat flux $\mathbf{q}$ only if the conductivity k and specific heat c_p are not function of temperature or if the average values for these quantities are used when the dependency on temperature exists. For most steels, the thermo-physical properties are temperature dependent. If this kind of dependency is considered, all properties should be updated at the beginning of each time step, which is time consuming especially for large size models. Moreover, such changes in properties would not be very large and would not significantly change the magnitude of $\mathbf{X}$. Also, updating the material properties at the beginning of each time step would be based on the temperatures $\mathbf{T}^{k^*}$ obtained from the initially given values of heat flux $\mathbf{q}^*$, which is essentially an approximation. The assumption of using a constant value is, therefore, justified. As a slight modification to the above assumption, we may opt for updating the sensitivity matrix $\mathbf{X}$ every M steps (in our numerical experiments, $M = 10$). Both methods led to similar results and the use of constant sensitivity matrix is justified.

Other factors affecting the accuracy of the calculated heat fluxes are the future information and the addition of regularization parameters. To improve the accuracy due to these factors, iterative technique with convergence limits is adopted in this study.

Now we consider some modifications to Eq. (15). The term $\alpha \mathbf{q}^*$ (eventually would be $\alpha^n \mathbf{q}$ in the iterative process) would lead to an increment $\Delta^1 \mathbf{q}$ and a better estimation for first value of the first heat flux ${}^1\mathbf{q}$. The term makes the calculation more cumbersome with very little benefit in convergence and, therefore, will be neglected and the equations may be written as:

$$(\mathbf{X}^{\mathrm{T}}\mathbf{X}+\alpha\mathbf{I})\Delta^{1}\mathbf{q}=\mathbf{X}^{\mathrm{T}}\Delta\mathbf{T}^{*} \tag{18a}$$

$${}^{1}\mathbf{q}=\mathbf{q}^{*}+\Delta^{1}\mathbf{q} \tag{18b}$$

$$(\mathbf{X}^{\mathrm{T}}\mathbf{X}+\alpha\mathbf{I})\Delta^{n}\mathbf{q}=\mathbf{X}^{\mathrm{T}}\Delta^{n-1}\mathbf{T} \tag{18c}$$

$${}^{n+1}\mathbf{q}={}^{n}\mathbf{q}+\Delta^{n}\mathbf{q} \tag{18d}$$

where n is the number of iterations.

2.2.3.2. Sequential technique and function specification. Starting with either Eq. (15) or Eq. (18), a number of N flux vectors $\mathbf{q}^{i}$ for $i=1,\ldots,N$ corresponding to each time step considered can be estimated simultaneously. When N is equal to the whole time step in the measurement, the developed method may theoretically be used to obtain the time history of heat fluxes.

The focus of this study is, however, more on the application of the method than on the method itself. During water jet cooling process, the temperature at each measurement point will sharply drop only within few limited time steps. Such sharp drop means large load or heat flux vector would occur during such small fraction of the time domain. Other measuring points will have the same phenomena but at different time window. This means that there will be large fluctuation in the load vector and the convergence of the solution may be significantly affected.

The number of time steps N is normally less than 10. A "computation window" of size N may be used sequentially for the determination of heat fluxes in the overall span of considered time for the analysis. To clarify this procedure, an example is illustrated in the following where we use $N=3$ at the beginning of the analysis. At the first sequence, the heat fluxes at the first three steps may be obtained by iteration as:

$${}^{n+1}\begin{pmatrix}\mathbf{q}^{1}\\ \mathbf{q}^{2}\\ \mathbf{q}^{3}\end{pmatrix}={}^{n}\begin{pmatrix}\mathbf{q}^{1}\\ \mathbf{q}^{2}\\ \mathbf{q}^{3}\end{pmatrix}+{}^{n}\begin{pmatrix}\Delta\mathbf{q}^{1}\\ \Delta\mathbf{q}^{2}\\ \Delta\mathbf{q}^{3}\end{pmatrix} \tag{19}$$

The subsequent three heat flux vectors $\mathbf{q}^{4}$ to $\mathbf{q}^{6}$ may be estimated if the temperatures $\mathbf{T}^{3}$ are considered as initial temperature. Then the computation window moves three steps for each subsequent sequence.

The above procedure presents a hybrid approach between a whole domain one and a true sequential one (will be addressed later in this work). This hybrid method implies that the heat fluxes at the previous iteration at each time step would be used in the next iteration for the corresponding time step, i.e., at the $n+1$ iteration ${}^{n}\mathbf{q}^{1}$ will be used for the first time step, ${}^{n}\mathbf{q}^{2}$ for the second one and ${}^{n}\mathbf{q}^{3}$ for the third one and there will be no need for function specification.

In this paper, a completely sequential approach with function specification is used. First, the newly calculated ${}^{n}\mathbf{q}^{1}$ is used for all time steps in the computation window after the first iteration, i.e., constant function specification is used for this computation window. Second, the computation window moves one time step at the next sequence after obtaining a convergent solution in the current sequence. Once again using the previous example, the first computation window consists of time step 1 to time step 3; and the second one includes time step 2 to time step 4.

2.2.3.3. Convergence norm. In each time step, the iterative procedure is used until the inversely predicted temperature $\mathbf{T}_{\mathrm{c}}$ converges to the measured temperature $\mathbf{T}_{\mathrm{m}}$. Convergence criteria used to define the acceptance of the predicted temperature are based on an error norm defined by:

$$\text{Error-norm}^{n}=\|\Delta\mathbf{T}^{n}\| \tag{20}$$

Two convergence criteria for ending the iteration process at each time step are used:

$$\text{Error-norm}^{n}\leqslant\delta T \tag{21a}$$

or

$$\frac{|\text{Error-norm}^{n+1}-\text{Error-norm}^{n}|}{\text{Error-norm}^{n}}\leqslant\varepsilon \tag{21b}$$

The values of δT and ε depend on the measurement error level. The rational behind using absolute criteria is that while the norm at a given previous iteration is already very small, the relative norm criterion is still not satisfied at last iteration.

2.2.4. Flowchart

Fig. 2 shows a simplified flowchart for the IHCP solution procedure presented. In the above procedure, the initial guess $\mathbf{q}^{*}$ of heat flux $\mathbf{q}$ may be taken as zero or any other value. However, the heat flux $\mathbf{q}^{2}$ obtained at the previous sequence may be used as the initial guess of heat flux at the current step to accelerate and enhance convergence.

Numerical parametric test results indicated that such setup of the initial guess of heat flux is better than a random guess, and that in inverse calculation the fluctuation of inversely calculated heat flux due to random error in

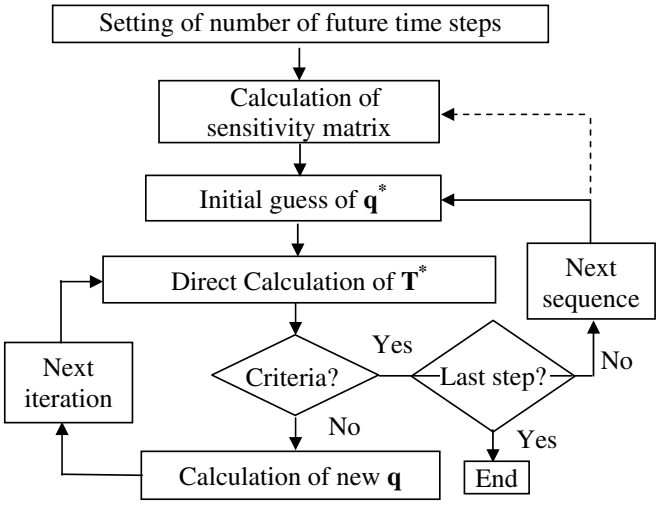

Fig. 2. Flowchart for IHCP solution procedure.

the measurement data may be damped by increasing the number of future steps and regularization parameter. It was also shown that the inversely calculated heat flux will be fairly close to input values (within ±8%) if the convergence criterion for internal temperature is ±1 °C. This procedure is capable of providing a time profile of heat fluxes at multiple locations in a 2D highly transient problem with sufficient accuracy [26].

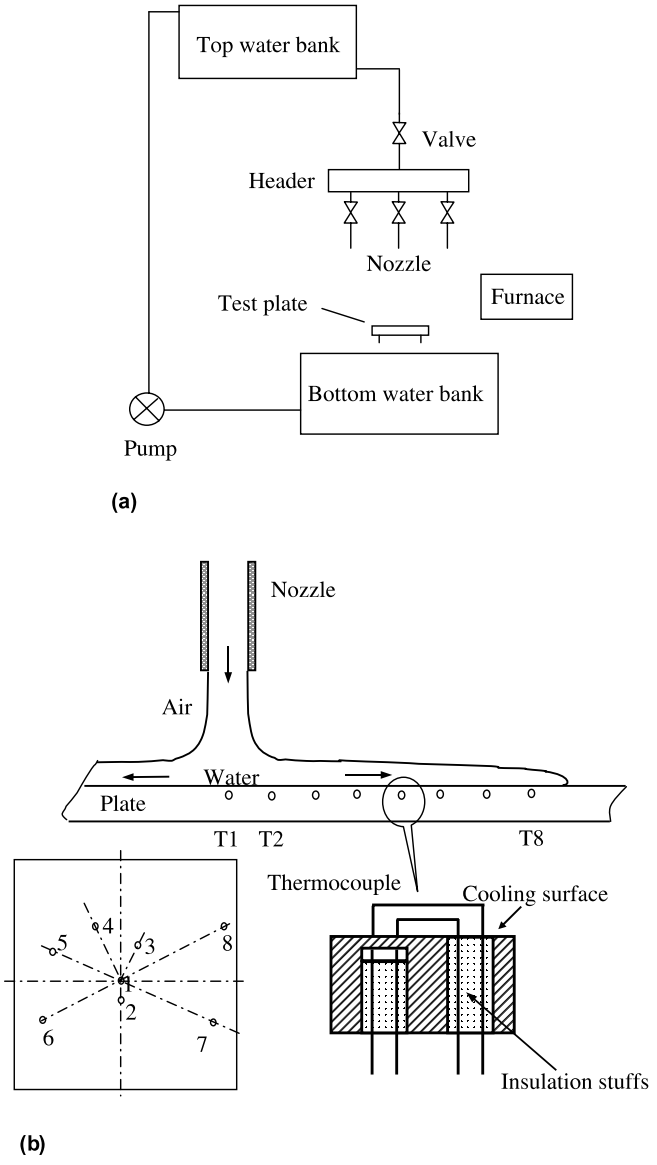

Fig. 3. Schematic diagram of experiment setup at UBC: (a) ROT test facility; (b) arrangements of thermocouples.

3. Experimental setup and experiments

3.1. Test facility

As schematically shown in Fig. 3a, the industry-scaled facility consists of a top and a bottom water banks, a top header and a bottom header (not shown), a water pump and pipe circuits and flow control valves, a furnace and apparatuses (not shown) for heating water and measuring water temperatures.

Three nozzles can be setup onto the top header and can be easily changed as necessary. Nozzle dimensions are compatible with those used in steel industry. The distance between the top nozzles is adjustable from 50 mm to 90 mm. The spike or the vertical distance of the top nozzle exit to the test plate can be also adjusted from 0.6 m to 2 m. The top nozzles are used for top surface cooling [21–24] (discussion in this paper is focused on the top surface cooling). Only one bottom nozzle (not shown) is available and its alignment or entry angle to the plate may be changed. This bottom nozzle is used for bottom surface cooling. Total water flow capacity has a maximum of 138 *l*/min. And the water can be heated to 90 °C. It should be noted that most of the abovementioned parameters are very close to those used in steel industry.

In all tests carried out and discussed below, only one nozzle is used. For stationary case, the nozzle is closed before the test plates are positioned at the designed location where the water should hit the centre of the test plates. Then the cooling water impinges onto the surface to be cooled. The electrical heating furnace has the capacity to heat test plates up to 1200 °C. Though, the initial temperatures of test plates are kept between 700 °C and 900 °C.

3.2. Test plates

The test plate dimensions are up to $280 \times 280 \times 10$ mm. Most of test plates have a nominal thickness of 7 mm. The materials of test plates are carbon steel DQSK and stainless steel SS316. The typical chemistries of DQSK and SS316 are listed in Table 1.

The density and specific heat of both steels are assumed to be constant and are 7800 kg/m^3 and 470 J/kg °C, respectively. For the conductivity of DQSK the following equation is assumed:

$$k = 60.571 - 0.03849 \times T\ (^\circ\mathrm{C}) \quad \text{in W/m}\,^\circ\mathrm{C} \tag{22}$$

The conductivity of SS316 is also slightly temperature dependent and the following equation is assumed:

$$k = 11.141 + 0.014 \times T\ (^\circ\mathrm{C}) \quad \text{in W/m}\,^\circ\mathrm{C} \tag{23}$$

Table 1
Chemical composition of steel plates used (wt%)

Steel	C	Mn	P	S	Si	Al	N	Cr	Ni	Mo
DQSK	0.06	0.24	0.005	0.011	0.006	0.041	0.0035			
SS316	0.03	1.86	0.045	0.030	1.0			19.2	11.3	2.67

Eqs. (22) and (23) are valid for the temperature ranging from 0 °C to 1200 °C.

3.3. Temperature measurements

With respect to the temperature measurements and the determination of surface flux or heat transfer coefficient, one of the common procedures used in literature is to use thermocouples on the opposite side of the plate or impeded below the top surface and to obtain the flux distribution on the surface through inverse analysis. In the experiments performed here, we use both surface and embedded thermocouples that are separated by a small distance, approximately 1 mm, and have pairs of two point measurements that may be used for the calculation of the surface flux distribution.

Thermocouples of Type K are used in all experiments. Thermocouples of Type K would normally have an error of approximately 2 °C or 0.75% of the target temperatures when used at a temperature lower or higher than 277 °C. Each of the thermocouple wires is around 0.051 mm (0.002″) in diameter and is insulated and sealed by a metallic protective coat that has an outer diameter of about 1.6 mm (1/16″).

As shown in Fig. 3b, a total of 16 thermocouples are used in each test and are installed at eight locations in the circumferential direction starting in the center of the plate with an increment of 15.9 mm (5/8″) in the radial direction. The thermocouples are numbered from 1 at center to 8 at the farthest point from the center. At each location, an internal thermocouple is installed in a blind hole with a diameter of 1.6 mm (1/16″) that is drilled from the bottom surface of the plate. The measuring junction is fixed onto the end surface of the hole that is about 1 mm (0.04″) below the top surface of the plate. A thickness-through hole of the same diameter is drilled with a centre distance of 3.2 mm (1/8″) from the blind hole. Another thermocouple is inserted in the through hole and its wires are spot welded on the top surface above the blind hole. It is to be noted that the thermocouple wires are separately welded to the designed locations, i.e. the separation junction is adopted. The distance of wire leads is approximately 1 mm.

3.4. Tests and procedure

The effects of steel grade, water temperature and water flow rate have been investigated. Twenty-seven tests are selected from more than 30 tests conducted and renumbered and listed with their corresponding parameters in Table 2. It should be noted that the initial plate temperatures are measured internally at the stagnation points at the very instant when the plates were pulled out from the heating furnace. The time of translating and setting up the plate from the heating furnace to the designed position of plate is not, normally, constant and this implies that the starting cooling temperature of plate may be slightly different even if the initial temperature is the same.

Table 2
Experimental conditions

Test	Steel	T_w, °C	Q_w, *l*/min
1–4	DQSK	30	15, 30, 30, 45
4–7	DQSK	40	15, 30, 45
8–10	DQSK	50	15, 30, 45
11–12	DQSK	60	15, 30
13–16	DQSK	70	15, 15, 30, 45
17–19	DQSK	80	15, 30, 45
20–24	SS316	30	15, 15, 30, 30, 45
25–27	SS316	50	15, 30, 45

Test plates were heated to the designed temperatures and then withdrawn from the heating furnace and transferred to the test position. The cooling water was turned on and impinged onto surface. The cooling times to room temperature varied greatly for different water temperatures. During the whole cooling process, the water flow rate and water temperature were maintained constant. The temperatures of plates at all measurement points were recorded with a rate of 100 Hz from the very instant when test plates were pulled out from the heating furnace.

To analyze the heat transfer behavior we need several hydrodynamic parameters besides the processing ones: jet velocity, jet diameter and saturation temperature of water. These parameters are listed in Table 3 and the following equations are used to calculate them.

The jet velocity (also called impact velocity) with which water vertically hits the plate can be calculated by

$$V_j = \sqrt{V_n^2 \pm 2gH} \tag{24}$$

where V_j is the jet velocity, m/s; V_n is the water velocity at nozzle exit, m/s; g is gravitational acceleration, m/s^2; and H is the vertical distance from nozzle exit to plate surface, m.

The diameter of water jet D_j is calculated by

$$D_j = D_n \cdot \sqrt{V_n / V_j} \tag{25}$$

where the D_n is nozzle diameter.

The pressure at the stagnation point is given by

$$P_s = P_a + \frac{1}{2}\rho V_j^2 \tag{26}$$

where P_a is the atmospheric pressure and ρ is the density of water.

The saturation temperature T_{sat} can be obtained from the saturation table of water according to the pressure.

Table 3
Hydrodynamic parameters at stagnation point

No.	Q_w, *l*/min	D_n, mm	V_n, m/s	D_j, mm	V_j, m/s	P_s, Pa	T_{sat}, °C
1	15	19	0.88	7.6	5.49	116,389	103.6
2	30	19	1.76	10.6	5.70	117,556	103.9
3	45	19	2.64	12.6	6.03	119,502	104.4

3.5. Measured temperature profiles

Typical measured temperature profiles are shown in Fig. 4. The cooling conditions for these two tests are almost identical but the steel grade is different. It is to note that the curves from left to right present the temperatures at thermocouple locations from T1 to T8, corresponding to those in Fig. 3b. Also the data shown in the figures and used in the inverse calculations is smoothed and filtered. A simple but effective 11-point average smoothing technique is used to filter noise in measured temperatures, that is, the average value of the temperature at a current time plus five prior values and five subsequent values was taken as the temperature at the current time step. Careful checks and comparisons showed that the random errors were less than ±1 °C and that all the features of the actual cooling curves were retained in the smoothed profiles and that the peak temperature gradients are not affected. It can be inferred that the calculated heat flux is of the accuracy of ±8%.

It may be seen from the two figures that at the air cooling stage the plate temperature is fairly uniform and it decreases gradually and almost linearly due to radiation and air convection heat transfer. As soon as the water impinges onto the plate, the temperatures at locations 1 and 2 have an immediate and remarkable drop and then the gradient decreases slightly, followed by a second sharp drop in temperature. It is to be noted that the cooling curves of temperatures at these two locations are almost identical for the whole cooling time for all tests considered. From a thermo-dynamical viewpoint, location 1 and 2 are within the boundaries of the impingement zone.

With the spreading of cooling water on the plate surface, the temperatures at locations 3–8 begin to decrease. However, the magnitude of the initial drop becomes smaller with increased distance from stagnation. It is worthy to point out that the temperature curves at all locations change their slopes to much smaller values when the temperature reaches about 200–400 °C.

Comparing Figs. 4a and b shows that the water front moves faster for stainless steel than for the DQSK. It takes about 27 s for the water to reach the last thermocouple for the SS316 as opposed to about 34 s for the DQSK. Also the two figures reveal that the slopes of curves start to level earlier for the SS316 than for the DQSK; the former takes place at around 400 °C whereas the latter appears at about 250 °C. The rational behind the influence of the steel grades on the cooling process is quite a complex topic and would be discussed in another paper.

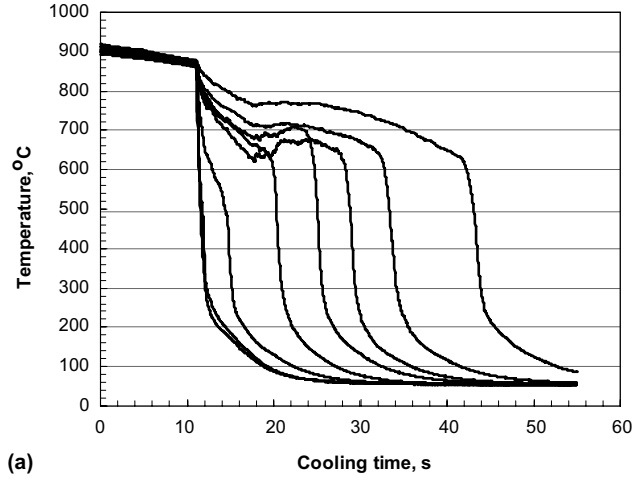

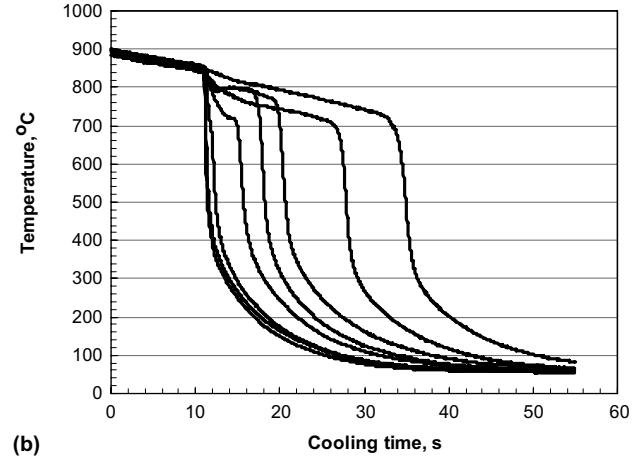

Fig. 4. Examples of measured cooling curves: (a) test 10; (b) test 27.

4. Application of the inverse method and result discussion

4.1. Heat flux profile

Before we focus on the heat transfer at the stagnation point, we present an overall view of heat fluxes on the top surface for one of the two tests for the DQSK, as shown in Fig. 5.

For the test, a full 2D axisymmetric FE model has been used. The model has 115 mm radius and 7 mm thickness.The model has 2430 quadratic elements with 4-nodes per element. The elements are uniform in the radial direction and vary from fine (on top surface) to coarse (on the

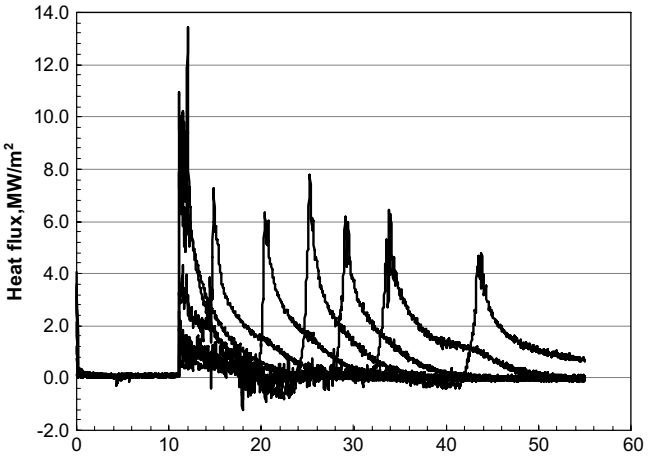

Fig. 5. Calculated heat fluxes for test 10.

bottom surface) in the thickness direction. In the calculations, constant average conductivity values of 31.5 W/m °C and phase transformation heat is not considered. The right hand surface, i.e., the outside of the cylindrical disc, is assumed thermally insulated and a constant heat flux equivalent to air cooling is applied to the bottom surface.

A simple and effective assumption of heat flux distribution on the top surface at each time step is performed as the following: the top surface is divided into eight sub-regions; each sub-region is symmetric with respect to the location of the corresponding thermocouple. The heat fluxes for all nodes in each individual sub-region are assumed to have the same value, i.e., there are only eight heat fluxes corresponding to the eight measurements locations. The actual values of heat fluxes at the eight points corresponding to measurements of temperatures are determined using inverse analysis. Only the data at the current time step is used and the regularization parameter is fixed at 1e−10. It is worth noting that with the above parameters, only several iterations were needed to get convergent results for each step.

The results in Fig. 5 actually reveal all features of its corresponding temperature curves. For the air cooling stage, the heat fluxes at all locations have relatively close values of about 14 kW/m^2, which is typical due to the combination of radiation and air convection cooling.

As the water hits the plate, the heat fluxes at locations 1 and 2 instantaneously jump to a very high value. For the tests using the DQSK there is a slight drop in the heat flux (after the initial jump corresponding to the initial drop in temperature) and then a second significant jump occurs. The flux profiles at these two locations are almost identical in shape with slight difference in values for all performed tests and times. The difference in heat fluxes comes from the slight difference in temperatures, which ascertains the sensitivity of the inverse problem. It is also noted that the peak value of heat flux is much higher for the SS316 than for the DQSK.

The heat fluxes at thermocouple locations 3–8 jump at different time instants proportional to the distance from the stagnation point when the cooling water first reaches the location. The shapes of heat flux profiles are, again, almost identical. The magnitudes of the highest heat fluxes at these locations are much lower than those at locations 1 and 2.

4.2. Effect of water temperature

The heat transfer in water jet impingement is a complex phenomenon that depends on many factors such as water temperature, water impinging velocity, plate surface temperature as well as the physical properties of both water and plate. It is generally believed that on the top surface, various conditions such as film boiling, transition boiling, nucleate boiling and single convective heat transfer may simultaneously occur. In the following section, the initial water temperature is from 30 °C to 80 °C and its effect on the heat transfer behavior at stagnation point is discussed.

Fig. 6 depicts the calculated surface temperature profiles at different water temperature levels for the DQSK. It should be noted that the starting time has been adjusted by shifting to allow the curves to be clearly separated for better comparison, and that the time interval for two adjacent points on the curves is the same and is equal to 0.1 s. It is clear that the surface temperature drops in several time steps to quite low temperature of around 300–200 °C as the cooling water of less than 50 °C impinges onto the plate surface and the cooling rate is as high as 2000–2400 °C/s. After this fast dropping stage the cooling process starts to level off. For a water temperature of higher than 60 °C, much more time is needed to cool the surface from around 880 °C to 200 °C, which can be verified by the point density at the higher temperature part of the curves.

The cooling curve at water temperature of 80 °C is quite different from the first two. When the cooling water hits the plate surface there is a fairly long and gentle cooling process, which implies that the cooling capacity is low. As

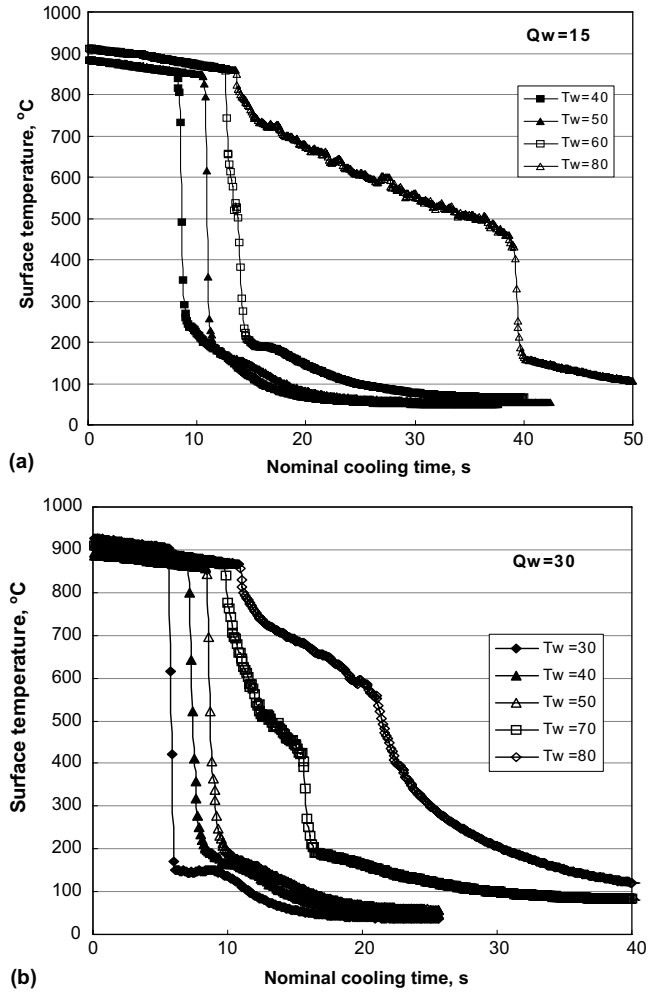

Fig. 6. Effect of water temperature on surface temperature: (a) $Q_w = 15$ *l*/min; (b) $Q_w = 30$ *l*/min.

the surface temperature reaches around 450 °C faster cooling stage appears and the surface temperature drops to around 200 °C in several time steps.

Fig. 7 shows the effect of water temperature on the cooling behavior for the DQSK. Take the results at water flow rate of 15 *l*/min for example. Generally, the heat flux is higher for lower water temperature than that for higher ones. The maximum or critical heat flux is around 14 MW/m^2 for water temperature of 40 °C and 6 MW/m^2 for water temperature of 80 °C. It may be concluded that increasing the water temperature significantly reduces the heat extraction from the plate. It should be pointed out that all critical heat flux values are higher than those predicted by Liu and Zhu [13] using the following equation:

$$q_{\text{critical}} = 0.36 \times (V_j/D_n)^{1/3} \tag{27}$$

where q_{critical} is the critical heat flux at stagnation zone, MW/m^2; V_j is the jet velocity, m/s; and D_n is the nozzle diameter, m. From the test conditions presented in this study, the critical values based on Eq. (27) are 2.38–2.46 MW/m^2.

Water temperature also affects the cooling pattern or thermodynamics. At lower water temperature (<50 °C), the heat flux monotonously increases with the decreasing of surface temperature until a value of about 300 °C and then again monotonously decreases with the decreasing of surface temperature. This may indicate that there is no film boiling regime at the beginning and the heat transfer is due to transition boiling and then it shifts to nucleate boiling. The rational behind this phenomenon is the sharp drop of surface temperature at the beginning and the incapacity to heat the water to the vaporization temperature. It may be concluded that the surface around the stagnation point is immediately wetted by water at lower water temperature.

Contrast to the situation at lower water temperature, there exists a film boiling regime when the water temperature is higher than 60 °C. When the cooling water of higher temperature impinges onto the surface, it is easily heated to boiling temperature and the heat flux is kept at a lower value. The duration of film boiling depends mainly on the water temperature in the test conditions. It is clear by comparing the boiling curve for 60 °C water temperature with that for 80 °C that the higher the water temperature, the longer the film boiling period and the lower the heat flux for this period.

From the above discussion we may postulate that the maximum water temperature for immediate wetting is around 60 °C, which is in good agreement with the theoretical prediction [14] that no film boiling occurs on stagnation point when the water with a temperature of higher than 60 °C hits the test plate whose temperature is lower than 900 °C, and with the finding reported in reference [15] where such a temperature is 68 °C.

It is worthy to point out the difference of the film boiling mode shown in Fig. 7a from that corresponding to water pool cooling. For the film boiling in water pool cooling, the heat flux decreases with the decrease of surface temperature to a minimum heat flux value. This feature was also reported in reference [16] for water jet cooling. In the case shown in Fig. 7a, the heat flux during the film boiling period does not change much and is nearly kept at a constant value. This trend is more obvious when the water temperature is 80 °C, i.e., the subcooling is around 20 °C.

The temperature at which the heat flux reaches its minimum value and the heat transfer shifts from film boiling to transition one is commonly referred as the Leidenfrost point. From Fig. 7a the Leidenfrost point is around 510 °C and 430 °C for water temperature of 60 °C and

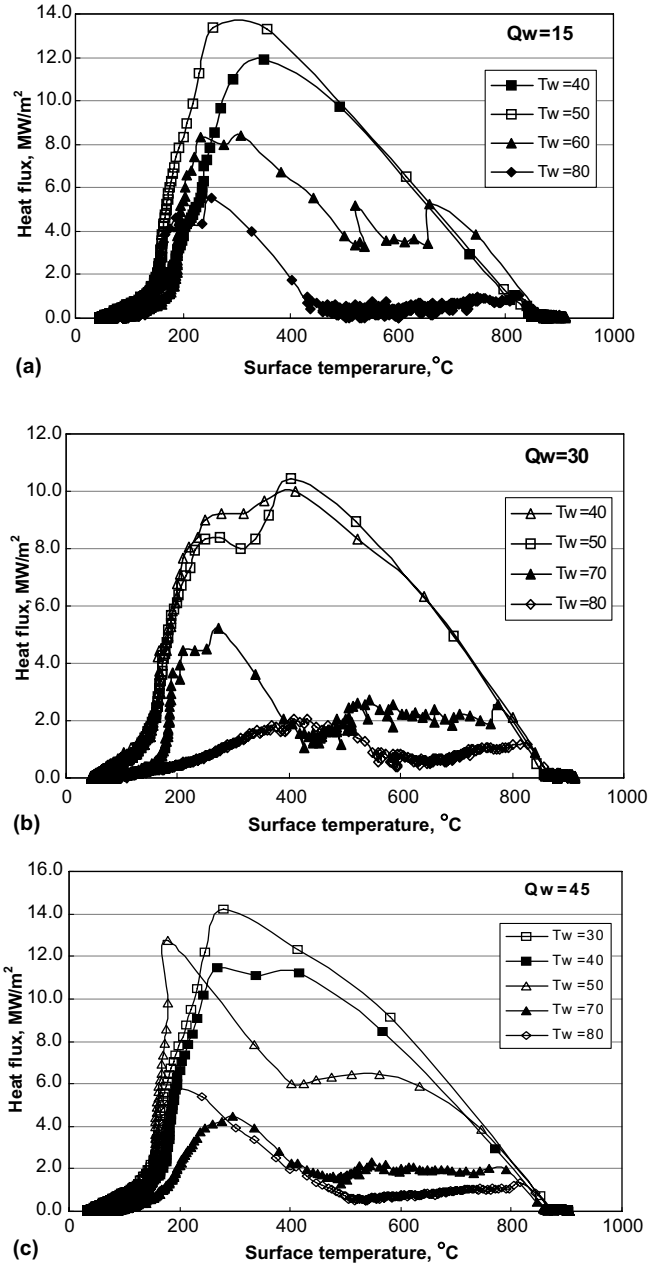

Fig. 7. Effect of water temperature on heat flux for DQSK: (a) $Q_w = 15$ *l*/min; (b) $Q_w = 30$ *l*/min; (c) $Q_w = 45$ *l*/min.

80 °C, respectively, which means that the Leidenfrost point shifts to higher value when the water temperature decreases.

Also the figure indicates that there is a single forced convection regime when the surface temperature is lower than about 150 °C where the slope of boiling curve changes from a mild one to a sharp one.

The results at flow rates of 30 *l*/min and 45 *l*/min are shown in Figs. 7b and c. These figures illustrate similar trends to that obtained for the lower flow rate of 15 *l*/min discussed above.

4.3. Effect of water flow rate

The impingement velocity is only proportional to the water flow rate when the distance of jet to the plate and the diameter of jet are fixed, as the conditions in this study. Thus, the effect of impingement velocity can be represented by the effect of water flow rate, as shown in Figs. 8 and 9. The two figures indicate somewhat different phenomenon; i.e., the water flow rate has little effect on heat transfer when water temperatures is 30 °C, 40 °C, 70 °C and 80 °C (Figs. 8a–d) but it has a noticeable effect when the water temperature is 50 °C (Fig. 9). This is a characteristic to be carefully checked.

It may be seen from Figs. 8a and b that the heat transfer regimes are sequentially transition boiling, nucleate boiling and convective boiling when the surface temperature decreases from 880 °C to room. There are some differences among the maximum heat flux values and the temperatures at which the maximum heat flux occurs when the water temperature is 30 °C. This difference does not appear when the water temperature is 40 °C.

It may be, generally, stated that the heat flux should increase with the increase in jet velocity because higher velocity increases the pressure as well as the saturation temperature of water at the stagnation and, therefore, the subcooling increases. In the test conditions presented, when the water flow rate varies from 15 *l*/min to 45 *l*/min, i.e., an increase of 3-fold, the jet velocity increases only from 5.49 m/s to 6.03 m/s and both pressure and saturation temperature show modest changes. Such small changes should not cause significant changes in heat flux. This point is also consistent with Eq. (27).

The above discussion may also be applied to the heat flux values at higher water temperatures, as shown in Figs. 8c and d. The difference among the boiling curves at lower and higher water temperature lies in the existence of film boiling regimes. For the film boiling regime, the heat flux decreases slightly with the decline of surface temperature. There is no clear and defined relationship between the Leidenfrost point and the water flow rate at different water temperature levels.

Although the boiling curve for water flow rate of 30 *l*/min shows the same combination of heat transfer modes as those for water flow rate of 15 *l*/min or 45 *l*/min, its

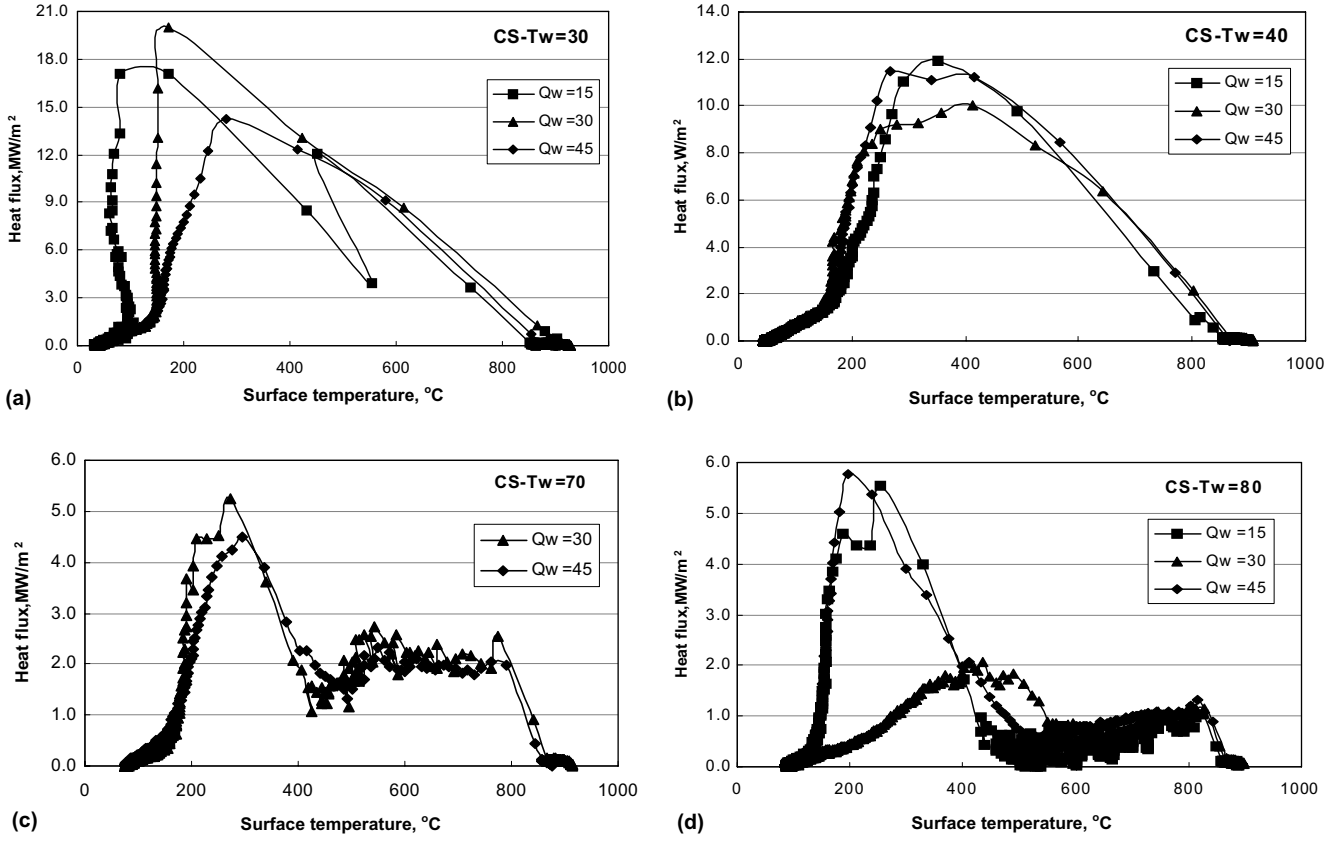

Fig. 8. Effect of water flow rate on heat flux for DQSK: (a) $T_w = 35$ °C; (b) $T_w = 40$ °C; (c) $T_w = 70$ °C; (d) $T_w = 80$ °C.

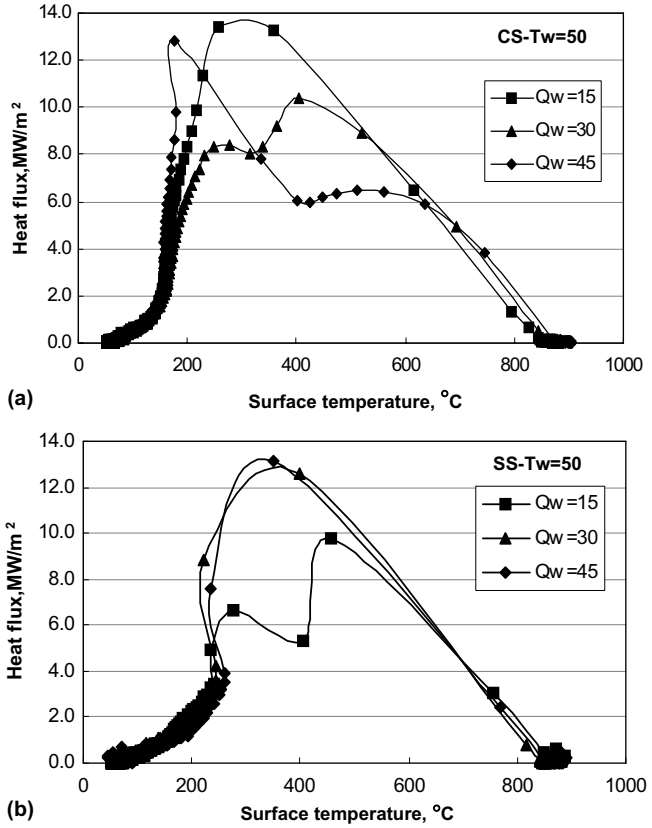

Fig. 9. Effect of water flow rate on heat flux at $T_w = 50$ °C: (a) DQSK; (b) SS316.

magnitude is much less than the values at corresponding points. Whether this may be attributed to measurement error or to a complex relationship at the higher temperature is an issue to be explored in the future work.

Fig. 9 shows the boiling curves at the stagnation for water temperature of 50 °C and different flow rates for the DQSK(Fig. 9a) and for the SS316 (Fig. 9b). It is clear from Fig. 9a that there is no a film boiling regime and that little effect of water flow rate can be observed at the beginning of the transition boiling region and the later period of the nucleate boiling. The higher effect of water flow rate occurs when the surface temperature varies from 600 °C to 200 °C. It is to be noted that this kind of effect is, generally, against to the common accepted trend, i.e., the increase of water flow rate does not increase the heat transfer capacity. This is quite abnormal and further investigation would be needed to verify the phenomenon.

Fig. 9b is used to clarify the effect of water flow rate on heat transfer behavior at water temperature of 50 °C for the SS316. It is clear that the maximum heat flux at water flow rate of 30 *l*/min or 45 *l*/min is higher than that at 15 *l*/min and that little effect can be seen for the overall cooling process for both flow rates of 30 *l*/min and 45 *l*/min.

From the above discussions we may conclude that the water flow rate generally has little effect on heat flux magnitude at all water temperature levels or subcooling levels. This may be attributed to the consideration that large variation of water flow rate has slight effect on the jet impinging velocity as well as the pressure and the saturation temperature. Also, it should be reported that some discrepancies are evident and further investigation is needed.

4.4. Effect of steel grade

The effect of steel grade on the heat transfer behavior is considered by the change in material properties, especially the heat conductivity in this study. Fig. 10a shows this kind of effect at water temperature of 30 °C. It can be seen that for two levels of water flow rates the heat fluxes with SS316 are always smaller than those with DQSK. The DQSK has generally higher conductivity than the SS316 and the difference in conductivities increases with the decline of temperature (refer to Eqs. (22) and (23)). When the temperature is around 500 °C, the conductivity of the DQSK is nearly twice that of SS316.

It incites the cooling effect of water at the plate surface and instigates faster decrease of the temperature at the target location. On the other hand, the heat from the bottom part is also easily transferred to the target location and this tends to increase the target temperature. To reduce the temperature at the target location to a same value, higher heat flux may be needed for cooling the material with higher conductivity. This may be the reason why the heat

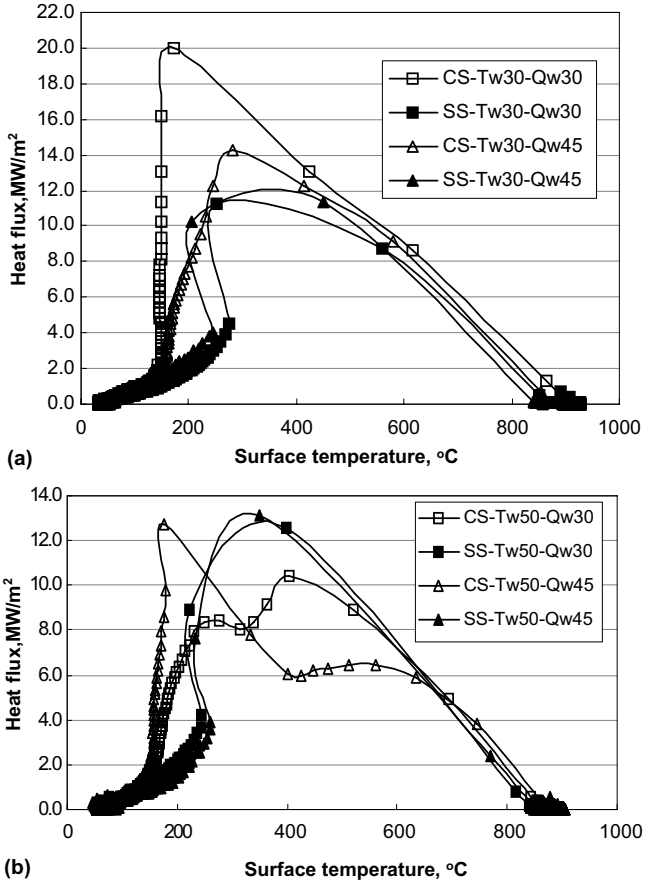

Fig. 10. Effect of steel grade on heat flux: (a) $T_w = 30$ °C; (b) $T_w = 50$ °C.

fluxes for the SS316 are always smaller than those for the DQSK for water temperature of 30 °C.

The effect of steel grade on heat flux at water temperature of 50 °C is shown in Fig. 10b. Contrast to the correlation at 30 °C, the heat fluxes for the SS316 are mostly higher than those for the DQSK for the same levels of water flow rates. As discussed above, the cooling capacity is mainly dependent on the water temperature and not the water flow rates. With the increase of water temperature, the cooling efficiency decreases. That means that the interior temperature decreases at a much lower rate with higher water temperature than with lower water temperature. Also, this indicates that the cooling is more confined at the top surface and it is easier to cool down the surface with higher conductivity than with lower conductivity, i.e., less heat flux is needed to reduce the surface temperature to a given value for the material with higher conductivity than for that with lower conductivity.

5. Summary

The heat transfer at the stagnation point or in impingement zone in circular water jet cooling is successfully determined by the inverse heat conduction procedure using iterative and sequential regularization method. The heat fluxes and surface temperature at the stagnation points of stationary plates cooled by an industry scale test facility are estimated by the IHCP method from the interior temperatures measured at around 1 mm below the plate surface. Analysis of data shows that the heat transfer behavior at the stagnation is mainly and greatly affected by water temperature, slightly affected by the steel grade and hardly affected by water flow rate. When the water temperature is lower than 60 °C the cooling process is governed by transition boiling, nucleate boiling and convective boiling. When the water temperature is higher than 60 °C, there is evidence of existence of a film boiling regime. The features of boiling curves and the typical values obtained are in good agreement with other resources. The results would contribute to better understanding of the controlled water cooling process in steel industry.

The presented method and procedure may be applied to solve nonlinear and highly transient inverse heat conduction problem with an acceptable level of accuracy.

Acknowledgements

The authors express their appreciation to Ms. M. Qi and Mr. A.T. Hauksson for their experimental data. This research has been funded through a strategic grant by the National Science and Engineering Research Council of Canada (NSERC).

Appendix A. Finite element matrix equations

The governing equation for conduction heat transfer in three-dimensional solid is given by:

$$\rho c\frac{\partial T}{\partial t}=\left[\frac{\partial}{\partial x}\left(k_x\frac{\partial T}{\partial x}\right)+\frac{\partial}{\partial y}\left(k_y\frac{\partial T}{\partial y}\right)+\frac{\partial}{\partial z}\left(k_z\frac{\partial T}{\partial z}\right)\right]+q^B \tag{A.1}$$

where k_x, k_y, k_z are the thermal conductivities in x, y and z directions, respectively, T is the temperature, q^B is the internal rate of heat generated per unit volume, t is the time, ρ is the density and c is the specific heat.

The above equation may be subject to the general form of the boundary conditions of:

$$k_n\frac{\partial T}{\partial n}=q^s+h(T_\mathrm{f}-T_\mathrm{s})+\varepsilon\sigma(T_\mathrm{sr}^4-T_\mathrm{s}^4) \tag{A.2}$$

where n is the normal to the boundary and the input heat flux is considered only on pertinent surfaces, i.e. surfaces that have specified boundary conditions and are given by: concentrated or distributed flux (q^s), convection BC; ($h(T_\mathrm{f}-T_\mathrm{s})$, h is the convection heat transfer coefficient, T_f is the fluid temperature and T_s is the surface temperature) and radiation BC; ($\varepsilon\sigma(T_\mathrm{r}^4-T_\mathrm{sr}^4)$, ε is the emissivity of the surface, σ is the Stefan–Boltzmann constant, T_sr is the absolute temperature of surface and T_r is the known temperature of the external radiative source).

The sources of nonlinearity in Eq. (A.1) may be due to temperature dependent material properties or dependency of the boundary conditions on temperature.

Eq. (A.1) may be re-written in the form:

$$\rho c\frac{\partial T}{\partial t}+\nabla\cdot\mathbf{q}-q^B=0 \tag{A.3}$$

where ∇ and $\mathbf{q}$ are defined as follows:

$$\nabla=\frac{\partial}{\partial x}\mathbf{i}+\frac{\partial}{\partial y}\mathbf{j}+\frac{\partial}{\partial z}\mathbf{k},\quad \mathbf{q}=[\,q_x\quad q_y\quad q_z\,]^\mathrm{T}$$

$$q_x=-k_x\frac{\partial T}{\partial x};\quad q_y=-k_y\frac{\partial T}{\partial y};\quad q_z=-k_z\frac{\partial T}{\partial z}$$

Table A.1
Definition of the terms in the FE general heat conduction equation

$[C]=\int_V \rho c[N]^\mathrm{T}[N]\,\mathrm{d}V$	Thermal capacity matrix
$[K_c]=\int_V [B]^\mathrm{T}[K][B]\,\mathrm{d}V$	Thermal conductivity matrix
$[K_h]=\int_S h[N^s]^\mathrm{T}[N^s]\,\mathrm{d}S$	Thermal conductivity matrix due to convection BC
$[K_r]=\int_S \kappa[N^s]^\mathrm{T}[N^s]\,\mathrm{d}S$	Thermal conductivity matrix due to radiation BC
$\{Q\}^b=\int_V q^B[N]^\mathrm{T}\,\mathrm{d}V$	Heat flux vector due to internal heat generation
$\{Q\}^s=\int_S q^s[N^s]^\mathrm{T}\,\mathrm{d}S$	Heat flux vector due to input surface flux
$\{Q\}^h=\int_S hT_\mathrm{f}[N^s]^\mathrm{T}\,\mathrm{d}S$	Heat flux vector due to convection BC
$\{Q\}^r=\int_S \kappa T_\mathrm{r}[N^s]^\mathrm{T}\,\mathrm{d}S$	Heat flux vector due to radiation BC
$\{T\}$, $\{\dot{T}\}$	Vector of global nodal temperatures and temperature gradients, respectively
$\kappa=\varepsilon\sigma(T_\mathrm{r}^2+T_\mathrm{sr}^2)(T_\mathrm{r}+T_\mathrm{sr})$	Equivalent heat transfer coefficient due to radiation
$\left\{\frac{\partial T}{\partial \mathbf{x}}\right\}=\frac{\partial}{\partial \mathbf{x}}(N_i\overline{T}_i)=[B]\{\overline{T}\}^e$	Partial derivative of temperature
$[K]=\begin{bmatrix}k_x & 0 & 0\\ & k_y & 0\\ \mathrm{sym} & & k_z\end{bmatrix}$	Element conductivity matrix
$[N]=[N_1\quad N_2\quad\cdots\quad N_n]$	Approximation or shape function, n is the number of nodes per element

Table A.2
Definition of the terms in heat transfer equation

Term	Name	Expression
${}^{t+\Delta t}\widehat{\mathbf{Q}}^{h^{(i-1)}}$	Nodal heat flux contribution due to convection BC, nonlinear and transient effects	${}^{t+\Delta t}\widehat{\mathbf{Q}}^{h^{(i-1)}} = \int_{S_h} {}^{t+\Delta t}h^{(i-1)}\mathbf{N}^{S^{\mathrm{T}}}\mathbf{N}^{S}({}^{t+\Delta t}\mathbf{T}_f - {}^{t+\Delta t}\mathbf{T}^{(i-1)})\,\mathrm{d}S$ *Note*: $\int_{S_h} {}^{t+\Delta t}h^{(i-1)}\mathbf{N}^{S^{\mathrm{T}}}\mathbf{N}^{S}\,\mathrm{d}S = {}^{t+\Delta t}\mathbf{K}^{h^{(i-1)}}$
${}^{t+\Delta t}\widehat{\mathbf{Q}}^{r^{(i-1)}}$	Nodal heat flux contribution due to radiation BC, nonlinear and transient effects	${}^{t+\Delta t}\widehat{\mathbf{Q}}^{h^{(i-1)}} = \int_{S_h} {}^{t+\Delta t}\kappa^{(i-1)}\mathbf{N}^{S^{\mathrm{T}}}\mathbf{N}^{S}({}^{t+\Delta t}\mathbf{T}_{\mathrm{r}} - {}^{t+\Delta t}\mathbf{T}^{(i-1)})\,\mathrm{d}S$ *Note*: $\int_{S_h} {}^{t+\Delta t}\kappa^{(i-1)}\mathbf{N}^{S^{\mathrm{T}}}\mathbf{N}^{S}\,\mathrm{d}S = {}^{t+\Delta t}\mathbf{K}^{r^{(i-1)}}$
${}^{t+\Delta t}\widehat{\mathbf{Q}}^{c^{(i-1)}}$	Nodal heat flux contribution due to conductivity, nonlinear and transient effects	${}^{t+\Delta t}\widehat{\mathbf{Q}}^{c^{(i-1)}} = \int_V \mathbf{B}^{\mathrm{T}}{}^{t+\Delta t}\mathbf{K}^{(i-1)}\mathbf{B}^{t+\Delta t}\mathbf{T}^{(i-1)}\,\mathrm{d}V$ *Note*: $\int_V \mathbf{B}^{\mathrm{T}}{}^{t+\Delta t}\mathbf{K}^{(i-1)}\mathbf{B}\,\mathrm{d}V = {}^{t+\Delta t}K^{C^{(i-1)}}$
${}^{t+\Delta t}\hat{\mathbf{q}}^{c^{(i-1)}}$	Nodal heat flux contribution due to thermal capacity, nonlinear and transient effects	${}^{t+\Delta t}\hat{\mathbf{q}}^{c^{(i-1)}} = \int_V {}^{t+\Delta t}(\rho c)^{(i-1)}\mathbf{N}^{\mathrm{T}}\mathbf{N}\cdot[({}^{t+\Delta t}\mathbf{T}^{(i-1)} - {}^{t}\mathbf{T})/\Delta t]\,\mathrm{d}V$ $\equiv {}^{t+\Delta t}\mathbf{C}^{(i-1)}[{}^{t+\Delta t}\mathbf{T}^{(i-1)} - {}^{t}\mathbf{T}]/\Delta t$

Now, we assume an approximation function for the temperature given by:

$$T(\mathbf{x}) = N_i(\mathbf{x})T_i \tag{A.4}$$

where $N_i(\mathbf{x})$ is the approximation function with i varying from one to the number of nodes per element, the vector $\mathbf{x}$ has the components x, y and z and T_i are the nodal temperature. Note that we consider only a typical element and assume that the normal finite element assembly procedures apply.

Applying Galerkin approach and utilizing Gauss theorem, the equivalent finite element equations representing Eqs. (A.1) and (A.2) may be written in the following final form:

$$[C]\cdot\{\dot{T}^e\} + [[K_c] + [K_h] + [K_r]]\cdot\{T^e\} = \{Q\}^b + \{Q\}^s + \{Q\}^h + \{Q\}^r \tag{A.5}$$

where the definitions of terms in Eq. (A.5) are summarized in Table A.1.

Considering the general nonlinear and transient case of Eq. (A.5), the solution may be realized by re-writing the equation at time $(t+\Delta t)$ and iteration (i) in the following form:

$${}^{t+\Delta t}\mathbf{C}^{(i)}{}^{t+\Delta t}\dot{\mathbf{T}}^{(i)} + {}^{t+\Delta t}(\mathbf{K}^c + \mathbf{K}^h + \mathbf{K}^r)^{(i)}{}^{t+\Delta t}\mathbf{T}^{(i)} = ({}^{t+\Delta t}\mathbf{Q}^b + {}^{t+\Delta t}\mathbf{Q}^s + {}^{t+\Delta t}\mathbf{Q}^h + {}^{t+\Delta t}\mathbf{Q}^r)^{(i)} \tag{A.6}$$

It may be shown that using Newton–Raphson approximation and the α-method, the solution to the above equation yields:

$${}^{t+\alpha\Delta t}\left[(\mathbf{K}^c + \mathbf{K}^h + \mathbf{K}^r) + \left(\frac{1}{\alpha\Delta t}\right)\cdot\mathbf{C}\right]^{(i-1)}\Delta\mathbf{T}^{(i)} = {}^{t+\alpha\Delta t}(\mathbf{Q}^b + \mathbf{Q}^s) + {}^{t+\alpha\Delta t}(\widehat{\mathbf{Q}}^h + \widehat{\mathbf{Q}}^r)^{(i-1)} - {}^{t+\alpha\Delta t}(\widehat{\mathbf{Q}}^c + \hat{\mathbf{q}}^c)^{(i-1)} \tag{A.7}$$

where the definition of the new terms introduced here are given in Table A.2.

References

[1] M. Korchynsky, Development of "controlled cooling practice", in: P.D. Southwick (Ed.), Accelerated Cooling of Steel, 1986, pp. 3–14.
[2] R.M. Guo, S.T. Hwang, Investigation of strip cooling behavior in the run-out section of hot strip mills, J. Mater. Process. Manufact. Sci. 4 (1996) 339–351.
[3] J. Filipovic, J. Viskanta, F.P. Incropera, A parameter study of the accelerated cooling of steel strip, Steel Res. 63 (1992) 496–499.
[4] D.H. Wolf, F.P. Incropera, R. Viskanta, Jet impingement boiling, Adv. Heat Transfer 23 (1992) 5–132.
[5] D.A. Zumbrunnen, F.P. Incropera, R. Viskanta, Method and apparatus for measuring heat transfer distributions on moving and stationary plates cooled by a planar liquid jet, Exp. Therm. Fluid Sci. 3 (1990) 202–213.
[6] T. Ochi, S. Nakanishi, M. Kaji, S. Ishigai, Cooling of a hot plate with an impinging circular jet, in: Multi-Phase Flow and Heat Transfer III, Proceedings of the Third Multi-Phase Heat and Flow Transfer Symposium Workshop, Miami Beach, FL, USA, April 18–20, 1983, pp. 671–681.
[7] S.J. Chen, J. Kothari, A.A. Tseng, Cooling of a moving plate with an impinging circular water jet, Exp. Therm. Fluid Sci. 4 (1991) 343–353.
[8] S.J. Chen, S.K. Biswas, A., Modeling and analysis of controlled cooling for hot moving metal plates, Monitoring and Control for Manufacturing Processes, American Society of Mechanical Engineers, Production Engineering Division (Publication) PED, vol. 44, 1990, pp. 465–474.
[9] J. Stevens, B.W. Webb, Local heat transfer coefficients under an axisymmetric, single-phase liquid jet, J. Heat Transfer 113 (1991) 71–78.
[10] N. Hatta, H. Osakabe, Numerical modeling for cooling process of a moving hot plate by a laminar water curtain, ISIJ Int. 29 (1989) 919–925.
[11] J. Filipovic, J. Viskanta, F.P. Incropera, Thermal behavior of a moving steel strip cooled by an array of planar water jets, Steel Res. 63 (1992) 438–446.
[12] H. Wolf, F.P. Incropera, R. Viskanta, Local jet impingement boiling heat transfer, Int. J. Heat Mass Transfer 39 (1996) 1395–1406.
[13] Z. Liu, Q. Zhu, Prediction of critical heat flux for convective boiling of saturated water jet impinging on the stagnation zone, Trans. ASME J. Heat Transfer 17 (2003) 159–165.
[14] Z. Liu, J. Wang, Study on film boiling heat transfer for water jet impinging on high temperature flat plate, Int. J. Heat Mass Transfer 44 (2001) 2475–2481.
[15] J. Kokado, N. Hatta, H. Takuda, J. Harada, N. Yasuhira, An analysis of film boiling phenomena of subcooled water spreading radially on a hot steel plate, Steel Res. 55 (1984) 113–118.
[16] S. Ishigai, S. Nakanishi, T. Ochi, Boiling heat transfer for plane water jet impinging on a hot surface, in: Proceedings of the Sixth

International Heat Transfer Conference, Toronto, Ont., Canada, August 1978.
[17] J.V. Beck, B. Blackwell, C.R.S. Clair Jr., Inverse Heat Conduction: Ill-posed Problem, Wiley Interscience Publication, New York, 1985.
[18] H.K. Kim, Evaluation of heat transfer coefficient during heat treatment by inverse analysis, J. Mater. Process. Technol. 112 (2001) 157–165.
[19] N. Al-Khalidy, A general space marching algorithm for the solution of two-dimensional boundary inverse heat conduction problems, Numer. Heat Transfer, Part B 34 (1998) 339–360.
[20] S.K. Kim, W.I. Lee, Solution of inverse heat conduction problems using maximum entropy method, Int. J. Heat Mass Transfer 45 (2002) 381–391.
[21] Z. Liu, D. Fraser, I.V. Samarasekera, Experimental study and calculation of boiling heat transfer on steel plates during runout table operation, Canad. Metall. Quart. 41 (2002) 63–74.
[22] Z. Liu, D. Fraser, I.V. Samarasekera, G.T. Lockhart, Experimental observation and modeling of thermal history within a steel plate during water jet impingement, Canad. Metall. Quart. 41 (2002) 75–86.
[23] A.T. Hauksson, Experimental study of boiling heat transfer during water jet impingement on a hot steel plate, Master Thesis, The University of British Columbia, 2001.
[24] Q. Meng, Experimental study of transient cooling of a hot steel plate by an impinging circular jet, Master Thesis, The University of British Columbia, 2002.
[25] K.H. Huebner, E.A. Thornton, T.G. Byrom, The finite element method for engineers, third ed., Wiley, New York, 1995.
[26] F. Xu, M.S. Gadala, A simple FE-inverse heat conduction algorithm and its application to the determination of surface heat flux during water jet cooling, in: Proceedings of the Fifth International Symposium on Multiphase Flow, Heat Transfer and Energy Conversion, July 3–6, Xi'an, 2005, China.